Check for updates

Tuning slow magnetic relaxation behaviour in a {Dy₂}-based one-dimensional chain *via* crystal field perturbation†

Shui Yu,[a] Qinhua Zhang,[c] Huancheng Hu,*[a] Zilu Chen, [ID]*[a] Dongcheng Liu,[a] Yuning Liang[a] and Fupei Liang [ID] *[ab]

Two novel {Dy₂}-based one dimensional chain compounds {[Dy₂(H₃L)₄(OAc)₆]·2MeOH}ₙ (**1**) and {[Dy₂(H₃L)₄(OAc)₄(NCS)₂]·2MeOH}ₙ (**2**) (H₃L = 1,3-bis(2-hydroxynaphthalenemethyleneamino)-propan-2-ol) have been prepared under solvothermal conditions. Crystal structure analyses indicate that **1** and **2** feature similar 1D chain structures bearing dinuclear secondary building units. The difference between these two structures is that one chelated acetate ligand of Dy(III) ion in **1** is replaced by one monodentate coordinated NCS⁻ ion in **2**, leading to their different coordination numbers and geometry configurations to Dy(III) ion. Magnetic properties indicate that **1** and **2** display slow magnetic relaxation behavior with an effective energy barrier of 16.44(2) K in **1** and 8.02(2) K in **2**, respectively, which is maybe attributed to the subtle crystal field perturbation of Dy(III) ions.

Introduction

Recently single-molecule magnets (SMMs) have attracted much attention because of their promising applications in ultrahigh-density information storage, molecular spintronic devices and quantum computing, *etc.*[1–3] Comparing with transition metal ions, lanthanide (Ln) ions often possess large orbital angular momentum and inherent magnetic anisotropy, which contribute to improving the effective energy barrier (U_{eff}) and blocking temperature (T_B) of SMM materials.[4–7] As a result, Ln ions particularly Dy(III) ion have become ideal candidates to construct SMM materials since Ishikawa *et al.* reported the first Ln-based SMM of [Pc₂Ln]⁻·TBA⁺ (Ln = Tb or Dy, Pc = dianion of phthalocyanine; TBA⁺ = N(C₄H₉)₄⁺) in 2003.[8] After that, numerous Ln-based SMM materials including discrete Lnₓ ($x \geq$ 1) coordination clusters, chainlike, two dimensional and three dimensional coordination compounds have been prepared and investigated in detail.[9–11]

Aiming at enhancing the performance of Ln-based SMM materials, many effective efforts have been dedicated by researchers in the past decades.[12–15] It is noteworthy that fine-tuning the symmetry of ligand field and/or the orientations of single-ion easy axes of lanthanide ions have been viewed as general and satisfactory approaches to increase the single-ion anisotropy of Ln(III) ions and further improve the values of U_{eff} and T_B of SMM materials.[16,17] For example, two essentially isomorphous planar {Dy₄} coordination clusters of [Dy₄(μ₃-OH)₂(hmmpH)₂(hmmp)₂Cl₄]·3MeCN·MeOH and [Dy₄(μ₃-OH)₂(hmmpH)₂(hmmp)₂(N₃)₄]·4MeOH {hmmpH₂ = 2-[(2-hydroxy-ethylimino)methyl]-6-methoxyphenol} exhibit an anion-dependent magnetic slow relaxation behavior.[18] When coordination water molecules in compound [Dy(acac)₃(H₂O)₂] are replaced by 1,10-phenanthroline or its derivatives with large aromatic groups, the energy barrier can also be enhanced.[19] Comparing with compound [Dy(H₂L)(NO₃)(H₂O)(EtOH)](NO₃)₂·H₂O (H₂L = 2,6-diylbis(ethan-1-yl-1-ylidene)di(isonicotinohydrazide)), the slow magnetic behavior of [Dy(L)(NO₃)(MeOH)₂] is changed obviously by deprotonating H₂L ligand and using different solvents.[20] Therefore, it is necessary to design and prepare compounds with similar or isomorphous structure by tuning ligands to control the anisotropy of Dy(III) ions and further explore the structure–property relationships of SMM materials. But up to now, the investigations of this field are still limited.

In this context, we report two polyhydroxylamine-derived Schiff-base {Dy₂}-based one dimensional chain compounds {[Dy₂(H₃L)₄(OAc)₆]·2MeOH}ₙ (**1**) and {[Dy₂(H₃L)₄(OAc)₄(NCS)₂]·

[a] State Key Laboratory for Chemistry and Molecular Engineering of Medicinal Resources, School of Chemistry and Pharmaceutical Sciences, Guangxi Normal University, Guilin 541004, P. R. China. E-mail: zlchen@mailbox.gxnu.edu.cn; siniantongnian@126.com; fliangoffice@yahoo.com

[b] Guangxi Key Laboratory of Electrochemical and Magnetochemical Functional Materials, College of Chemistry and Bioengineering, Guilin University of Technology, Guilin, 541004, P. R. China

[c] State Key Laboratory of Heavy Oil Processing, Institute of New Energy, College of Chemical Engineering, China University of Petroleum (East China), Qingdao 266580, P. R. China

$2MeOH\}_n$ (**2**) featuring with similar structures. The different coordination groups of Dy(III) in **1** and **2** lead to different geometrical configurations and symmetries and coordination numbers of Dy(III) ions. The slow magnetic relaxation behaviors of **1** and **2** are obviously perturbed by their difference of crystal field for Dy(III) ion. The energy barrier is 16.44(2) K and 8.02(2) K with pre-exponential factor of 3.25×10^{-6} s and 5.6×10^{-5} s in **1** and **2**, respectively.

Experimental

Materials and physical measurements

All chemicals were purchased from commercial companies and used directly without further purification. The Fourier transform infrared (FT-IR) data were collected on PerkinElmer Spectrum One FT-IR spectrometer using the corresponding KBr pellets in the wavenumber range of 4000–400 cm^{-1}. The powder X-ray diffraction (PXRD) measurements were carried out on a Rigaku D/max 2500v/pc diffractometer equipped with Cu-Kα radiation ($\lambda = 1.5418$ Å) at 40 kV and 40 mA, with a step size of 0.02° in 2θ and a scan speed of 5° min^{-1}. Elemental analyses for C, H and N elements were performed on an Elementar Micro cube C, H, N elemental analyzer. The TG analyses were conducted on a PerkinElmer Diamond TG/DTA thermal analyzer in a flowing nitrogen atmosphere with a heating rate of 5 °C min^{-1}. All magnetic data were measured on a Quantum Design MPMS SQUID-XL-7 SQUID magnetometer. The magnetic data were corrected with a consideration of diamagnetic contribution from the sample and the sample holder.

X-ray crystal structure analysis

The single crystal X-ray diffraction experiments were collected on SuperNova diffractometer with graphite monochromated Mo-Kα radiation ($\lambda = 0.71073$ Å). The single crystal structures were solved by the direct method using SHELXT[21] and refined by means of full-matrix least-squares procedures on F^2 by the SHELXL program.[22] All non-hydrogen atoms (C, N, O, S and Dy) were located by different Fourier maps and subsequently refined with anisotropic displacement parameters. The H atoms attached on C and N atoms were refined at the geometrical sites. The details of crystallographic data of **1** and **2** are presented in Table S1.† Selected bond lengths and bond angles in **1** and **2** are listed in Tables S2 and S3,† respectively.

Synthesis

Preparation of compound 1. A solution of H$_3$L (0.1 mmol, 0.0414 g) and Dy(OAc)$_3$·10H$_2$O (0.1 mmol, 0.0513 g) in methanol (1.5 mL) and acetonitrile (0.5 mL) was sealed in a Pyrex tube under vacuum and then the tube was heated at 80 °C for 3 days. The resulted clear yellow solution was placed at room temperature for evaporation to give pale yellow crystals after 3 days (yield 23% based on Dy(OAc)$_3$·10H$_2$O). Anal. calcd for C$_{64}$H$_{68}$Dy$_2$N$_4$O$_{20}$: C, 49.97; H, 4.46; N, 3.64%. Found: C, 49.84; H, 4.52; N, 3.73%. IR (KBr pellet, cm^{-1}): 3426 (m), 2919 (w), 2854 (w), 1634 (s), 1545 (m), 1448 (m), 1401 (m), 1436 (m), 1304 (m),

1194 (w), 1033 (w), 957 (w), 844 (w), 744 (w), 675 (w), 607 (w), 544 (w), 463 (w), 411 (m).

Preparation of compound 2. Methanol (1.5 mL) and acetonitrile (0.5 mL) were added in a Pyrex tube containing H$_3$L (0.1 mmol, 0.0414 g), KSCN (0.2 mmol, 0.0194 g) and Dy(OAc)$_3$·10H$_2$O (0.2 mmol, 0.1026 g). The tube was sealed under vacuum and heated at 80 °C for 3 days. The resulted clear yellow solution was placed at room temperature for 3 days, and the pale yellow crystals were collected (yield 28% based on Dy(OAc)$_3$·10H$_2$O). Anal. calcd for C$_{62}$H$_{66}$Dy$_2$N$_6$O$_{16}$S$_2$: C, 48.34; H, 4.32; N, 5.46%. Found: C, 48.56; H, 4.50; N, 5.36%. IR (KBr pellet, cm^{-1}): 3425 (s), 2923 (w), 2850 (w), 2053 (m), 1635 (s), 1545 (m), 1459 (m), 1387 (s), 1307 (w), 1194 (w), 1112 (w), 1033 (w), 954 (w), 820 (w), 755 (w), 672 (w), 476 (w).

Results and discussion

Structural characterization

Crystal structure of compound 1. Single crystal X-ray diffraction analysis revealed that **1** crystallizes in triclinic crystal system $P\bar{1}$ space group. The asymmetric unit of **1** contains one crystallographically independent Dy(III) ion, one H$_3$L ligand, three OAc$^-$ ions and one lattice methanol molecule. Dy(III) ion is coordinated by nine O atoms from two H$_3$L ligands and four carboxylate groups, giving a distorted muffin coordination geometry with C_s symmetry by SHAPE analysis (Table S4†). Two adjacent Dy(III) ions with the distance of 4.120 Å are bridged by two bidentate carboxylate oxygen atoms to form a dinuclear [Dy$_2$O$_2$] unit, and these [Dy$_2$O$_2$] units are further connected by H$_3$L ligands to form 1D chain structure (Fig. 1d). The Dy(III)–O bond distances range from 2.285(2) to 2.564(3) Å and Dy–O–Dy bond angles are in the range of 49.70(12)° to 148.94(12)°.[23,24]

Crystal structure of compound 2. Single crystal X-ray diffraction analysis implies that the structure of **2** is similar to **1** except for one chelated carboxylate group of central Dy(III) ion in **1** replaced by one NCS$^-$ ion in **2**, leading to the different
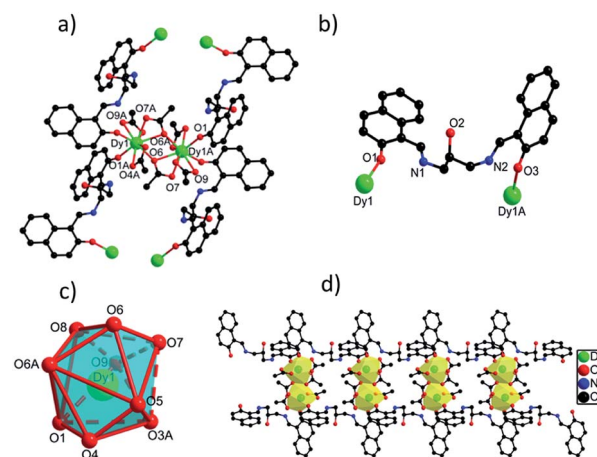

Fig. 1 (a) The structure of {Dy$_2$} core in **1** with selected atoms labelled. (b) The coordination mode of H$_3$L ligand in **1**. (c) The coordination polyhedron of Dy(III) ion in **1**. (d) The 1D chain structure of **1**.

coordination numbers and geometry configurations of Dy(III) ions in **1** and **2**. Similar to **1**, **2** as well crystallizes in triclinic crystal system $P\bar{1}$ space group. The asymmetric unit of **2** contains one crystallographically independent Dy(III) ion, one H$_3$L ligand, two carboxylate groups, one SCN$^-$ ion and one lattice methanol molecule. As depicted in Fig. S2,† the Dy(III) ion in **2** is coordinated by seven O atoms from two H$_3$L ligands and three carboxylate groups and one N atom from one SCN$^-$ ion, showing a triangular dodecahedron with D_{2d} symmetry by SHAPE analysis (Table S5†). Two neighboring Dy(III) ions with the distance of 4.027 Å are bridged by two O atoms from two carboxylate groups to form a [Dy$_2$O$_2$] unit, which are further linked to build 1D chain structure *via* bridging H$_3$L ligands (Fig. 2d). The bond lengths of Dy(III)–O and Dy(III)–N are in the range of 2.270(4)–2.501(5) Å, and the angles of O–Dy(III)–O and O–Dy(III)–N range from 51.63(14) to 165.86(17)°.[20,25] Interestingly, although different {Dy$_2$} units exist in **1** and **2**, they still exhibit similar 1D chain structures owing to the same bridging H$_3$L ligands. The flexibility of H$_3$L ligand leads to its slightly different coordination modes in **1** and **2**, thus they show different crystal packing structures which are constructed from the one-dimensional chains through $\pi\cdots\pi$ interaction rooting from aromatic rings (Fig. S1†).

Powder X-ray diffraction and thermogravimetric analysis

The experimental powder X-ray diffraction (PXRD) patterns of **1** and **2** match well with the corresponding simulated ones obtained from the single crystal X-ray diffraction data, respectively, confirming the high purity of the bulk samples of **1** and **2** (Fig. S3†). As shown in Fig. S4,† the thermogravimetric analysis (TGA) curve of **1** shows an obvious weight loss of 5.90% before 131 °C, due to the loss of MeOH molecules (calcd: 4.20%). With the temperature increasing, a platform is occurred before the collapse of the structure of **1** above 214 °C. The TGA curve of **2** exhibits a gradual weight loss of 4.75% below 248 °C, which is as well attributed to the loss of MeOH molecules (calcd: 4.20%). As
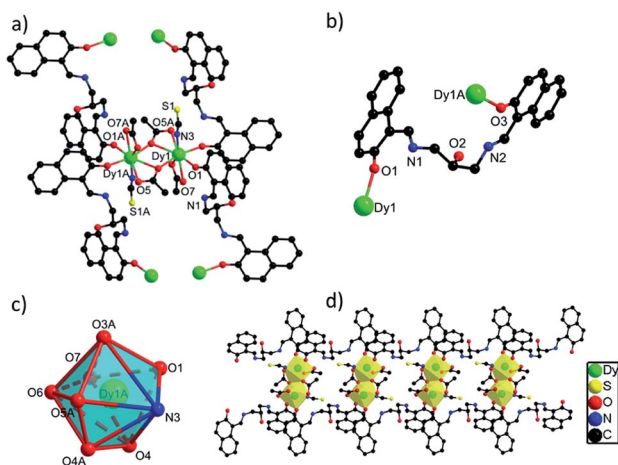
the temperature is further increased, the structure of **2** starts to decompose.

Magnetic properties

Direct current magnetic susceptibility measurements on polycrystalline samples of compounds **1** and **2** were performed in the temperature range of 1.8–300 K under an external field of 1000 Oe. As shown in Fig. 3, the $\chi_M T$ values at room temperature of **1** and **2** are 26.73 and 29.47 cm^3 K mol^{-1}, which are very close to the theoretical value of 28.34 cm^3 K mol^{-1} for two uncoupled Dy(III) ion ($^6H_{15/2}$, $L = 5$, $g = 4/3$).[26,27] For compound **1**, the $\chi_M T$ value gradually decreases in the temperature range of 300 K to 178 K. Upon cooling, the value of $\chi_M T$ in **1** decreases rapidly and reaches a minimum of 22.36 cm^3 K mol^{-1} at 1.8 K. For compound **2**, the $\chi_M T$ value almost keeps constant up to 161 K, and then it reduces rapidly to 21.92 cm^3 K mol^{-1} at 1.8 K. The behavior of **1** and **2** at low temperature can be attributed to thermal depopulation of excited Stark sub-levels, antiferromagnetic interactions between Dy(III) ions and/or large magnetic anisotropy of Dy(III) ions (Fig. 3 and 4).

The field-dependent magnetization for **1** and **2** at 1.8, 2.5, 5.0 and 10 K exhibit that the magnetization increases rapidly in the low field, and then slowly increases with the increasing applied field. The maximum values of *M* for **1** and **2** at 7 T are obviously lower than the theoretical saturated value of 20 Nβ for dinuclear Dy(III) compounds (Fig. S5†).[28,29] Meanwhile, the non-superposition of the *M vs. H/T* plots for **1** and **2** at different temperatures in the high field further implies that the above mentioned behavior is probably due to the crystal-field-induced splitting of the Stark level, significant magnetic anisotropy and/or low-lying energy states.[30–32]

In order to investigate the dynamic magnetic properties of compounds **1** and **2**, variable frequency alternating current (ac) magnetic susceptibilities were firstly performed with 3 Oe alternating field and 0 Oe direct current (dc) field at 2 K. No peaks are observed in the in-phase (χ') *vs. ν* and out-of-phase (χ'') *vs. ν* curves for **1** and **2**, which may be attributed to the presence of quantum tunneling of magnetization (QTM). To suppress the QTM effect, different dc fields ranging from 200 to 4000 Oe were applied on **1** and **2**, unfortunately, no obvious peaks were observed in χ' *vs. ν* and χ'' *vs. ν* plots for **1** and **2** (Fig. S7 and S8†). Therefore, for **1** and **2**, the alternating current magnetic susceptibilities measurements were measured in the frequency range of 1–1000 Hz under zero dc field. As shown in Fig. 5, clear frequency dependence and temperature dependence of χ'' signals can be
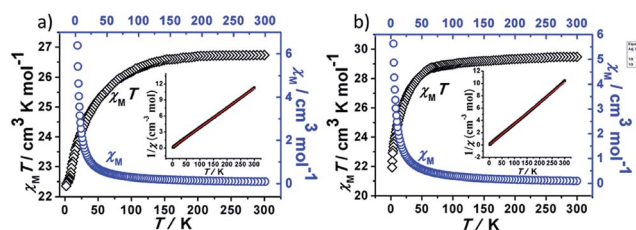

Fig. 2 (a) The structure of {Dy$_2$} unit in **2** with selected atoms labelled. (b) The coordination mode of H$_3$L ligand in **2**. (c) The coordination polyhedron of Dy(III) ion in **2**. (d) The 1D chain structure of **2**.

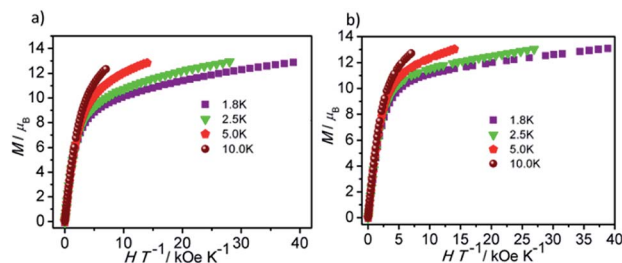Fig. 3 Plots of χ_M and $\chi_M T$ *vs. T* for **1** (a) and **2** (b).

Fig. 4 Plots of M vs. HT^{-1} for **1** (a) and **2** (b) measured at 1.8, 2.5, 5.0 and 10 K.
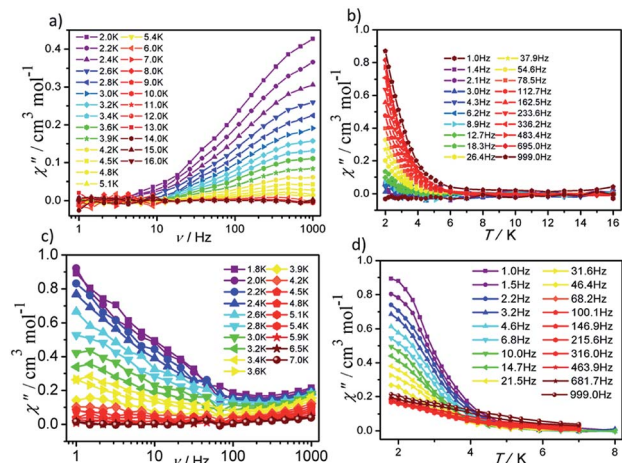

Fig. 5 Frequency- and temperature-dependent out-of phase (χ'') ac susceptibilities for **1** (a and b) and **2** (c and d) under zero dc field.

observed although no obvious peaks were detected in **1** and **2**, illuminating the existence of typical slow magnetic relaxation processes in **1** and **2**. The obvious difference of χ' signals vs. temperature plots and frequency dependencies plots for **1** and **2** (Fig. S9 and S10†) maybe derive from their different coordination numbers and geometry configurations and symmetries of the central Dy(III) ion.

The effective energy barrier (U_{eff}) and relaxation time (τ_0) of **1** and **2** can be obtained by fitting $\ln(\chi''/\chi')$ vs. $1/T$ data with the following equation: $\ln(\chi''/\chi') = \ln(\omega\tau_0) + E_a/(k_BT)$,[33–35] and the excellent linear fitting between $\ln(\chi''/\chi')$ and $1/T$ can be depicted at different frequencies, yield $U_{eff} \approx 16.44$ K and 8.02 K, $\tau_0 \approx$
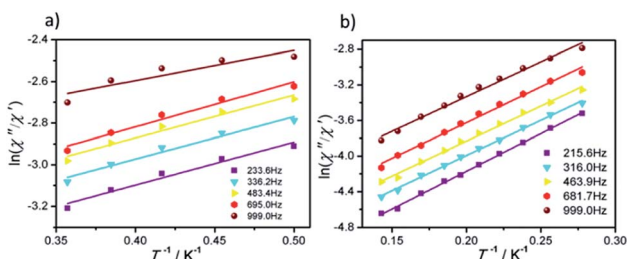

Fig. 6 Plots of $\ln(\chi''/\chi')$ vs. $1/T$ for **1** (a) and **2** (b) under 0 Oe dc field, the solid lines represent the best fits.

3.25×10^{-6} s and 5.6×10^{-5} s for **1** and **2**, respectively. The different effective energy barrier and relaxation time for **1** and **2** are due to the different anisotropy of their Dy(III) ions from subtle crystal field perturbation caused by the change of one chelated acetate in **1** by one NCS$^-$ ligand (Fig. 6).

Conclusions

In conclusion, two new {Dy$_2$}-based 1D chain structures bearing a Schiff-base ligand were constructed and characterized in detail. Magnetic properties indicate that they exhibit similar slow magnetic relaxation behavior under zero dc field. Interestingly, one chelated acetate ligand in **1** is replaced by one NCS$^-$ ion in **2**, which leads to the different coordination geometries of their Dy(III) ions, and thus their different Dy(III) anisotropies. All of these factors results in their different effective energy barriers. This phenomena indicates that the slight crystal field perturbation of Dy(III) ions will affect the slow magnetic behavior for the compounds with similar structures. This work will enrich the methods of tuning the performance of SMM materials via crystal field perturbation effect.

Conflicts of interest

There are no conflicts to declare.

Acknowledgements

References

1 L. Ungur, S.-Y. Lin, J. Tang and L. F. Chibotaru, *Chem. Soc. Rev.*, 2014, **43**, 6894–6905.

2 D. N. Woodruff, R. E. Winpenny and R. A. Layfield, *Chem. Rev.*, 2013, **113**, 5110–5148.

3 J. Liu, Y. C. Chen, J. L. Liu, V. Vieru, L. Ungur, J. H. Jia, L. F. Chibotaru, Y. Lan, W. Wernsdorfer, S. Gao, X. M. Chen and M. L. Tong, *J. Am. Chem. Soc.*, 2016, **138**, 5441–5450.

4 Y.-X. Wang, Y. Ma, Y. Chai, W. Shi, Y. Sun and P. Cheng, *J. Am. Chem. Soc.*, 2018, **140**, 7795–7798.

5 B. S. Dolinar, D. I. Alexandropoulos, K. R. Vignesh, T. James and K. R. Dunbar, *J. Am. Chem. Soc.*, 2018, **140**, 908–911.

6 M. K. Singh and G. Rajaraman, *Inorg. Chem.*, 2019, **58**, 3175–3188.

7 A. Bhanja, R. Herchel, Z. Travnicek and D. Ray, *Inorg. Chem.*, 2019, **58**, 12184–12198.

8 N. Ishikawa, M. Sugita, T. Ishikawa, S.-y. Koshihara and Y. Kaizu, *J. Am. Chem. Soc.*, 2003, **125**, 8694–8695.

9 Z.-H. Zhu, X.-F. Ma, H.-L. Wang, H.-H. Zou, K.-Q. Mo, Y.-Q. Zhang, Q.-Z. Yang, B. Li and F.-P. Liang, *Inorg. Chem. Front.*, 2018, **5**, 3155–3162.

10 A. B. Canaj, M. Siczek, M. Otreba, T. Lis, G. Lorusso, M. Evangelisti and C. J. Milios, *Dalton Trans.*, 2016, **45**, 18591–18602.

11 J. Kobylarczyk, M. Liberka, P. Konieczny, S. Baran, M. Kubicki, T. Korzeniak and R. Podgajny, *Dalton Trans.*, 2020, **49**, 300–311.

12 L. F. Chibotaru, L. Ungur and A. Soncini, *Angew. Chem., Int. Ed.*, 2008, **47**, 4126–4129.

13 J. Mayans, Q. Saez, M. Font-Bardia and A. Escuer, *Dalton Trans.*, 2019, **48**, 641–652.

14 Y. N. Guo, G. F. Xu, W. Wernsdorfer, L. Ungur, Y. Guo, J. Tang, H. J. Zhang, L. F. Chibotaru and A. K. Powell, *J. Am. Chem. Soc.*, 2011, **133**, 11948–11951.

15 A. A. Patrascu, M. Briganti, S. Soriano, S. Calancea, R. A. Allao Cassaro, F. Totti, M. G. F. Vaz and M. Andruh, *Inorg. Chem.*, 2019, **58**, 13090–13101.

16 R. J. Blagg, C. A. Muryn, E. J. McInnes, F. Tuna and R. E. Winpenny, *Angew. Chem., Int. Ed.*, 2011, **50**, 6530–6533.

17 F. Habib, P. H. Lin, J. Long, I. Korobkov, W. Wernsdorfer and M. Murugesu, *J. Am. Chem. Soc.*, 2011, **133**, 8830–8833.

18 Y.-Z. Zheng, Y. Lan, C. E. Anson and A. K. Powell, *Inorg. Chem.*, 2008, **47**, 10813–10815.

19 G.-J. Chen, Y.-N. Guo, J.-L. Tian, J. Tang, W. Gu, X. Liu, S.-P. Yan, P. Cheng and D.-Z. Liao, *Chem.–Eur. J.*, 2012, **18**, 2484–2487.

20 J. Wang, H. Wang, Y. Ma, J. Tang, L. Li, Q. Wang, B. Zhao, P. Cheng and J. Ma, *Cryst. Growth Des.*, 2019, **19**, 3365–3371.

21 G. Sheldrick, *Acta Crystallogr., Sect. A: Found. Crystallogr.*, 2008, **64**, 112–122.

22 G. Sheldrick, *Acta Crystallogr., Sect. C: Struct. Chem.*, 2015, **71**, 3–8.

23 S.-D. Jiang and S.-X. Qin, *Inorg. Chem. Front.*, 2015, **2**, 613–619.

24 K. Griffiths, P. Kumar, G. R. Akien, N. F. Chilton, A. Abdul-Sada, G. J. Tizzard, S. J. Coles and G. E. Kostakis, *Chem. Commun.*, 2016, **52**, 7866–7869.

25 H. L. Wang, X. F. Ma, J. M. Peng, Z. H. Zhu, B. Li, H. H. Zou and F. P. Liang, *Inorg. Chem.*, 2019, **58**, 9169–9174.

26 S. Biswas, L. Mandal, Y. Shen and M. Yamashita, *Dalton Trans.*, 2019, **48**, 14096–14102.

27 H. Ke, W. Wei, Y. Yang, J. Zhang, Y. Q. Zhang, G. Xie and S. Chen, *Dalton Trans.*, 2019, **48**, 7844–7852.

28 K. H. Zangana, E. Moreno Pineda and R. E. Winpenny, *Dalton Trans.*, 2015, **44**, 12522–12525.

29 W. Cao, C. Gao, Y. Q. Zhang, D. Qi, T. Liu, K. Wang, C. Duan, S. Gao and J. Jiang, *Chem. Sci.*, 2015, **6**, 5947–5954.

30 J. Lu, X.-L. Li, Z. Zhu, S. Liu, Q. Yang and J. Tang, *Dalton Trans.*, 2019, **48**, 14062–14068.

31 J. Vallejo, J. Cano, I. Castro, M. Julve, F. Lloret, O. Fabelo, L. Canadillas-Delgado and E. Pardo, *Chem. Commun.*, 2012, **48**, 7726–7728.

32 Q. Zhou, F. Yang, D. Liu, Y. Peng, G. Li, Z. Shi and S. Feng, *Inorg. Chem.*, 2012, **51**, 7529–7536.

33 M. J. Liu, J. Yuan, Y. Q. Zhang, H. L. Sun, C. M. Liu and H. Z. Kou, *Dalton Trans.*, 2017, **46**, 13035–13042.

34 H. Li, J. Sun, M. Yang, Z. Sun, J. Tang, Y. Ma and L. Li, *Inorg. Chem.*, 2018, **57**, 9757–9765.

35 I. A. Kühne, K. Griffiths, A.-J. Hutchings, O. P. E. Townrow, A. Eichhöfer, C. E. Anson, G. E. Kostakis and A. K. Powell, *Cryst. Growth Des.*, 2017, **17**, 5178–5190.